International Journal of Biological Macromolecules 322 (2025) 146538

Contents lists available at ScienceDirect

International Journal of Biological Macromolecules

journal homepage: www.elsevier.com/locate/ijbiomac

Structural-mechanistic insights and performance engineering of chitinase MpChit35 for tailored chito-oligosaccharide production

Marina Minguet-Lobato [a,c], Ángela Fernández-García [b], Elena Jiménez-Ortega [b,1], Fadia V. Cervantes [c], Pilar Sánchez-Pozo [a,2], Francisco J. Plou [c], Julia Sanz-Aparicio [b,*], María Fernández-Lobato [a,*]

[a] Department of Molecular Biology, Centre for Molecular Biology Severo Ochoa (CBM-CSIC-UAM), University Autonomous from Madrid. C/ Nicolás Cabrera, 1. Cantoblanco. 28049 Madrid, Spain
[b] Institute of Physical Chemistry Blas Cabrera (IQF-CSIC), C/ Serrano, 119, 28006 Madrid, Spain
[c] Institute of Catalysis (ICP-CSIC), C/ Marie Curie, 2. Cantoblanco. 28049 Madrid, Spain

ARTICLE INFO

Keywords:
Chitinase
Enzyme engineering
Structure-function relationship

ABSTRACT

Chitinase-catalysed synthesis offers a promising biotechnological route for converting chitin-rich waste into value-added chito-oligosaccharides, whose biological activity depends on their degree of polymerization and acetylation, highlighting the need for precise enzymatic tools to tailor their structures. This study investigates the structural-functional determinants of the chitinase MpChit35 from *Metschnikowia pulcherrima*, which mainly produces di-acetyl-chitobiose ($(GlcNAc)_2$) and to a lesser extent tri-acetyl-chitotriose ($(GlcNAc)_3$) from chitin. Here the MpChit35 structure was solved at 2.55 Å and structural analysis combined with site-directed mutagenesis enabled the identification of key residues involved in substrate binding and catalysis. Thus, the L253R mutation significantly increased the protein catalytic efficiency and promoted near-exclusive production of $(GlcNAc)_2$ from chitin and oligomeric substrates, underscoring the role of polar interactions in defining the enzyme specificity and processivity. In contrast, the multiple-mutation A107D/D151N/A181S/M279A favoured the release of $(GlcNAc)_3$ and tetra-acetyl-chitotetraose. Furthermore, residue Trp73 contributed to an unusual distal substrate-binding platform and Ala107 resulted a key determinant for the product specificity. These findings provide mechanistic insights into chitinase function and support the rational design of enzymes with tailored cleavage patterns. This work contributes to the development of efficient biocatalysts for sustainable chitin valorisation and the industrial production of custom chito-oligosaccharides.

1. Introduction

Chitin, the second most abundant polysaccharide in nature after cellulose, is a crucial structural component of fungal cell walls, arthropod exoskeletons, and various marine organisms. Despite its widespread occurrence, the efficient degradation and utilization of chitin remain challenging due to its highly crystalline and recalcitrant nature [1]. The accumulation of chitin-rich waste, particularly from seafood processing industries, poses significant environmental concerns, making the development of efficient biocatalytic processes for chitin valorisation an urgent biotechnological priority [2].

Chitinases of the glycosyl hydrolase family 18 (GH18) catalyse chitin hydrolysis into chito-oligosaccharides (COS), playing a key role in chitin turnover and attracting significant biotechnological interest [3,4]. COS are bioactive molecules with promising applications in agriculture, biomedicine, food and energy industries, owing to their antimicrobial, immunostimulatory, and prebiotic properties [5–8]. For instance, *N*-acetyl-D-glucosamine (GlcNAc) and di-acetyl-chitobiose ($(GlcNAc)_2$) could be employed in the bioethanol production [9]. Additionally hexaacetyl-chitohexaose ($(GlcNAc)_6$) has been shown to enhance the activity of natural killer cells in the spleen and promote the release of inflammatory cytokines [5], highlighting its immunomodulatory potential in pharmaceuticals. COS larger than $(GlcNAc)_2$ can act as biological resistance elicitors in plants, enhancing their defence against

* Corresponding authors.
E-mail addresses: xjulia@iqf.csic.es (J. Sanz-Aparicio), maria.fernandezlobato@uam.es (M. Fernández-Lobato).
[1] Present address: Spanish National Research Council (CNIO). C/ Melchor Fernández Almagro, 3, Spain.
[2] Present address: Centre for Plant Biotechnology and Genomics (CBGP-UPM-CSIC). Montegancedo Campus. 28,223, Pozuelo de Alarcón, Madrid, Spain.

https://doi.org/10.1016/j.ijbiomac.2025.146538
Received 24 April 2025; Received in revised form 22 July 2025; Accepted 1 August 2025
Available online 5 August 2025

infections and biotic stress [7], which underpins their agricultural applications. Furthermore, tetra-acetyl-chitotetraose ($(GlcNAc)_4$) is being explored as potential anti-diabetic agent [10]. All these examples emphasize the importance of the relationship between the chemical structure and the functionalities of these oligosaccharide types. However, the precise control of chitin degradation to generate specific COS types remains a significant technological challenge. Current industrial processes to produce COS often rely on harsh chemical hydrolysis methods, which are generally inefficient, environmentally detrimental, and lack selectivity. In contrast, enzymatic approaches mediated by chitinases offer a more sustainable alternative. Nevertheless, optimizing enzyme performance, specificity, selectivity and processivity is essential for their application in the controlled synthesis of COS from chitin, with precise degree of polymerization and acetylation for specific applications [11–14].

The overall structure of GH18 chitinases features a catalytic domain with a distinctive $(\beta/\alpha)_8$-barrel topology that contains at least two highly conserved sequences, DxDxE at the end of the β4-strand, including the catalytic acidic residues, and SxGGx at the β3-strand of the barrel [3,15]. Some GH18 chitinases contain an additional chitinase insertion domain (CID). Originally identified in bacteria, these enzymes are often referred to as bacterial-type chitinases. Structurally, the CID comprises five or six antiparallel β-strands and a single α-helix, inserted within the $(\beta/\alpha)_8$-barrel, specifically between the β7-strand and α7-helix [16,17]. In contrast, plant-type chitinases, which lack the CID, differ significantly from their bacterial counterparts in both, structure and function, particularly in their modes of action (endo/*exo*-action). Bacterial-type chitinases, which have been extensively studied, often exhibit highly processive *exo*-activity patterns. This is facilitated by a long and deep substrate-binding groove, partially formed by the CID and lined with multiple solvent-exposed aromatic residues. Examples of such exo-chitinases include SmChiA from *Serratia marcescens* and ThChit42 from *Trichoderma harzianum* [4,17–19]. Plant-type chitinases generally exhibit an *endo*-activity pattern, primarily due to their shallower substrate-binding cleft and the presence of a single solvent-exposed aromatic residue, which is commonly associated with reduced processivity. A representative example is the *endo*-chitinase ThChit33 from *T. harzianum* [20,21]. However, structural classification does not always reliably predict enzymatic function. A notable example is the human chitinase HCHT, which, despite having a typical *exo*-chitinase structure, functions as an *endo*-chitinase and exhibits processive behaviour [4,22]. Similarly, the *endo*-chitinase SmChiC from *S. marcescens* displays an atypical cleavage pattern, generating $(GlcNAc)_2$ when hydrolysing chitin and oligomeric substrates [15,19,23]. These cases underscore the complexity of the structure-function relationship in chitinases, highlighting the importance of both structural characterisation and bioengineering approaches for optimizing their functionality. A deeper understanding of these enzymes is crucial for assessing their potential applications in chitin valorisation.

Three newly characterised chitinases from the ubiquitous yeast *Metschnikowia pulcherrima*, MpChit35, MpChit38, and MpChit41, have been studied, with their structural models obtained using AlphaFold2 [24]. MpChit41 features a CID and an extended array of aromatic residues forming the active-site groove, characteristic of *exo*-acting bacterial-type chitinases. In contrast, MpChit35 and MpChit38 lack the CID and contain a highly conserved tryptophan (Trp281 in both cases), a hallmark of plant-type *endo*-acting chitinases. However, and despite their high sequence and structural similarity (sharing nearly 80 % sequence identity), MpChit35 and MpChit38 exhibit distinct enzymatic behaviours on chitin. MpChit35, which shows the greatest activity on the polysaccharide [24], acts as an *exo*-acting chitinase producing primarily $(GlcNAc)_2$, whereas MpChit38 acts as an *endo*-acting chitinase, generating mainly tri-acetyl-chitotriose ($(GlcNAc)_3$) [24]. Understanding this functional divergence is critical to optimize these enzymes for chitin bioconversion.

In this study, we investigate the structural and functional implications of targeted amino acid positions in MpChit35, aiming to refine its catalytic profile for more efficient and controlled chitin hydrolysis.

2. Materials and methods

2.1. Materials

α-Chitin (from shrimp shells, coarse flakes), *N*-acetyl-D-glucosamine (GlcNAc) and 4,4′-dicarboxy-2,2′-biquinoline dipotassium salt were obtained from Sigma Aldrich (St. Louis, MO, USA). Fully acetylated chito-oligosaccharide (*fa*COS) standards, including di-acetyl-chitobiose ($(GlcNAc)_2$), tri-acetyl-chitotriose ($(GlcNAc)_3$), tetra-acetyl-chitotetraose ($(GlcNAc)_4$), penta-acetyl-chitopentaose ($(GlcNAc)_5$) and hexa-acetyl-chitoheaxaose ($(GlcNAc)_6$) were from Megazyme (Bray, Irland). Colloidal chitin (CC) was prepared as previously described [18]. Basically, 10 g chitin in 10 M HCl was maintained 16 h at 4 °C, filtered through glass thick fibres into ethanol and then chitin floccules were precipitated at 4 °C, collected (5000 ×*g* during 10 min) and maintained in 0.1 M sodium acetate pH 4.0–4.5. Yeast Nitrogen Base w/o amino acids (YNB) was obtained from Difco (BD, Sparks, MD, USA). All reagents were of the highest purity grade.

2.2. Strains, expression media, plasmids, and site-directed mutagenesis

Escherichia coli DH5α was utilized as host for DNA manipulations using the standard techniques. *Komagataella phaffii* GS115 (also *Pichia pastoris* GS115; *his*4-, Mut+, Invitrogen, Carlsbad, CA, USA) was used as host for protein expression. Yeasts were maintained at 4 °C on YEP solid medium (glucose 2 %, yeast extract 1 %, peptone 2 %, agar 2 %; all *w/v*). The *K. phaffii* competent cells were prepared following the specifications of the manufacturers (Invitrogen), and transformants were selected on MD medium (YNB 1.34 %, glucose 2 %, biotin 0.04 %). BMG and BMM media (both MD, 0.1 M potassium phosphate pH 6.0 and glycerol 4 % or methanol 0.5 %, respectively) were used for growing transformants and analysing heterologous protein expression. Yeasts were cultured at 30 °C with orbital shaking (200 rpm), and growth was monitored spectrophotometrically at a wavelength of 600 nm (OD600).

The genes *mpChit35* and *mpChit38* from *M. pulcherrima* CECT 12827 (IFI 1205) of 1017 and 1083-bp (GenBank accession number: OR941418 for *mpChit35* and OR941419 for *mpChit38*), including the stop codon, encode proteins of 338 and 360 amino acidic residues (GenBank accession number: WVD50414.1 and WVD50415.1), respectively. Plasmids pIB4-MpChit35 and pIB4-MpChit38, containing the genes *mpChit35* and *mpChit38*, fused to the 267-bp sequences for the mating factor-α (*MF*α) from *Saccharomyces cerevisiae*, as secretion signal, and the methanol strong regulated alcohol oxidase 1 promoter (*AOX1*p) were previously obtained [24] and used as templates to obtain all the protein variants generated in this work. Production of all protein variants (MpChit35 and its variants and MpChit38) was induced by methanol as their expression was controlled by the *AOX1* promoter. Site-directed mutagenesis was carried out using the strategy described by Liu and Naismith in 2008 [25] with Phusion High-Fidelity DNA polymerase (NEB, Ipswich, UK) following the manufacturer recommendations and specific primers (Table S1) synthetised at IDT (Coralville, United States), which included rational designed mutations for substitutions W73D, A107D, S108Y, D151A/N, E153A, A181S, G252D/S, L253Q/R, M279A and D151A/E153A. Multiple-mutant variants were generated using the suitable template of specific simple mutants. The PCR reactions were treated with *Dpn*I to eliminate the parental plasmid and transformed into *E. coli*. Point mutations were verified by DNA sequencing using universal AOX1 and AOX2 primers (Table S1) at Macrogen (Madrid, Spain). DNA plasmids were extracted with NZYMiniprep kit (NzyTech, Lisbon, Portugal). Integrity of the constructions were also verified by DNA sequencing (Macrogen, Madrid, Spain). Constructions including the desired mutations were linearized with *Stu*I (New England Biolabs, NEB,

Herts, UK); into *HIS4* locus of the pIB4 derivatives and included in *K. phaffii* by electroporation according to the manual for protein expression in *Pichia* (Invitrogen, Carlsbad, CA, USA). Transformant were confirmed by colony PCR using universal AOX primers, and finally the heterologous protein expression of the selected transformants was conducted as previously described [24]. Briefly, selected colonies were transferred from MD agar plates into 25 mL of medium BMG (250 mL flaks) and cultivated at 30 °C and 250 rpm until reaching log-phase growth, about 4–8 units at OD600. Cells were collected by centrifugation (1500 ×*g*, 5 min), cultivated for 120 h in 200 mL of BMM (in 1 L flaks), and the induction of the protein expression conducted by adding 0.5 % methanol every 24 h. The culture growth was periodically evaluated at 600 nm and their pH maintained (if required) using 1 M potassium phosphate pH 6.0. Cells were removed (1500 ×*g* 5 min), extracellular fractions filtered using 0.22 μm membranes (Merck Life Science, Madrid, Spain).

Proteins produced by the yeast transformant were evaluated in sodium dodecyl sulphate-polyacrylamide gels (SDS-PAGE, 12 %) and stained with BlueSafe (NzyTech, Lisbon, Portugal). Precision Plus Protein Standards Unstained 10–250 kDa (Bio-Rad, Madrid, Spain) were used as molecular weight markers. Protein levels were assessed at 280 nm in a NanoDrop ND-1000 Spectrophotometer V3.8 (ThermoFisher Scientific Inc., Madrid, Spain) using bovine serum albumin as standard or quantified by densitometry of SDS-PAGE gels with the ImageJ Software Version 1.53 t. Protein were deglycosylated using PNGase F or EndoH (both from New England Biolabs, NEB, Herts, UK) in denaturing or non-denaturing conditions, respectively, according to the instruction of manufacturer.

2.3. Hydrolytic activity analysis

α-Colloidal chitin (CC) degradation was assessed by measuring the formation of reducing sugars using the bicinchoninic acid (BCA) method [26]. Briefly, reactions were carried out in a total volume of 400 μL containing 100 μL of enzyme solution, in a VorTemp 56 Shaking Incubator (LabNet, Madrid, Spain) at 900 rpm under previously established optimal reaction conditions (45 °C; pH 4.5 for MpChit35 and its variants, pH 4.0 for MpChit38) in 0.1 M sodium acetate [24]. When necessary, reaction volumes were scaled proportionally while maintaining the initial substrate-to-enzyme ratios. Reactions were terminated at 100 °C for 10 min, and the residual substrate was removed by centrifugation (11,000 ×*g*, 10 min, 4 °C). A standard curve of GlcNAc (0–0.3 g/L) was used. One unit of activity (U) was defined as that corresponding to the release of 1 μmol of reducing sugars per minute. Specific activity was determined using 10 g/L of CC substrate, and the apparent Michaelis-Menten kinetic constants were determined using 0 to 35 g/L CC substrate. Initial velocities were calculated from the linear phase of product formation and established by preliminary time-course assays. Curve plotting and analysis were performed using GraphPad Prism 9.0 Software (GraphPad Software, Boston, Massachusetts USA), with kinetic parameters calculated by fitting the initial rate values to the Michaelis-Menten equation. Based on their sequences, the theoretical molecular weights of proteins MpChit35 and MpChit38 were 34,890.15 Da and 38,330.86 Da, respectively, data that were used to calculate their molar concentrations. All reactions were performed in triplicate, and standard errors were calculated.

The reaction products from hydrolysis of $(GlcNAc)_n$ ($n = 2$, 3, 4 or 6) were determined by high-performance liquid chromatography (HPLC) with evaporative light scattering detection (ELSD). Reactions were performed in a solution containing 0.8–1 mM substrate and enzyme concentrations of 20 nM for $(GlcNAc)_6$ hydrolysis, and 100 nM for $(GlcNAc)_4$ hydrolysis using MpChit35, MpChit38, the MpChit35 D151N, A181S, and A107D/D151N/A181S/M279A (multiple) variants, and 5 nM for the L253R, M279A, and A107D variants. These enzyme concentrations correspond to an activity range of 0.1–1.5 mU/mL on CC. The reactions were carried out in 10.0 mM sodium acetate at pH 4.0 and 45 °C. Reactions were terminated by mixing each aliquot with an equal volume of 70 % (*v*/v) acetonitrile. A 10 μL sample of each reaction was injected into an HPLC system, equipped with a quaternary pump (mod. 600E, Waters Corp.), a Luna 5 μm NH2 100 Å column (250 × 4.6 mm), and a 4 × 3.0 mm NH2 guard column from Phenomenex. ELSD detection (mod. SEDEX 55, Sedere, France) was carried out at 40 °C with an autosampler (mod. 717 Plus, Waters Corp.; Milford, USA). The analytes were separated using an isocratic method with a mobile phase of 72 % acetonitrile and 28 % MilliQ water, set to a flow rate of 0.7 mL/min over 20–60 min, depending on the reaction. Peaks were analysed using Millenium[32] software. Calibration curves for *fa*COS with polymerization degrees from 1 to 6 were constructed across the 0.1–1.2 mM range, yielding linear plots with R^2 values between 0.98 and 1.00. Data plotting and statistical analysis were conducted with GraphPad Prism software version 9.0.

To determine the conversion percentage of $(GlcNAc)_6$ to $(GlcNAc)_3$ + $(GlcNAc)_3$ at a given time point, half the molar amount of $(GlcNAc)_3$ was divided by the decrease in $(GlcNAc)_6$ M amount, then multiplied by 100 [27]. Enzyme preference for trimer versus dimer products was assessed by calculating the molar ratio of $(GlcNAc)_3$ to $(GlcNAc)_2$ at specific time points.

The reaction products from hydrolysis of CC (10 g/L) were also analysed by matrix-assisted laser desorption ionization-time of flight (MALDI-TOF) mass spectrometry (MS) after 24 h reaction, using a mass spectrometer with Ultraflex III TOF/TOF (Bruker, Billerica, MA, USA) and an NdYAG laser. Mixtures were first treated with high cat-ionic exchange resin to minimize ionization inhibition. Registers were taken in positive reflector mode, within external calibration and 20 g/L 2,5-dihydroxybenzoic in acetonitrile (3:7) as a matrix. Samples were mixed with the matrix in a 4:1 ratio and 0.5 μL were analysed. The acquisition range was from *m/z* 40–3000 Da, and as referred previously [24], at the Interdepartmental Research Service (SIdI) of the Autonomous University of Madrid (UAM). Reactions were performed using 50 μM of enzymes for 24 h, at optimal enzyme conditions (45 °C and pH 4.0–4.5) [24].

2.4. Crystallization and X-ray structural determination

MpChit35 was heterologously expressed in *K. phaffii*, purified to homogeneity and deglycosylated with Endo H, after which the sample was concentrated and diafiltrated with a 10 kDa filtration membrane. MpChit35 at a concentration of 3.55 mg/mL in buffer 25 mM Tris HCl pH 7.5, 5 mM NaCl was purified in a MonoQ column for anion exchange chromatography. After that, MpChit35 was diafiltrated to reduce its salt content and concentrated again to of 5.6 mg/mL.

Initial commercial crystallization conditions for wild-type MpChit35 were tested using an Oryx8 robot (Douglas Instruments) for micro batch screening and optimization in 96-well crystallization plates (Hampton Research). JBS Classic and PACT (Jena Bioscience) were used. Crystals were grown by the sitting-drop vapor diffusion method at 18 °C. Many crystals were obtained based on PEG of different sizes (1000, 1500 and 400) as main precipitant, the best plates growing from 22 to 30 % (*v*/v) PEG 4000 and 200 mM ammonium sulphate and protein:reservoir ratio of 1:1. Drop sizes were adjusted for each case. Afterwards, high-quality crystals grew in 22 % (v/v) PEG 4000, 100 mM magnesium chloride and 100 mM sodium acetate pH 4.6. For data collection, crystals were cryoprotected with 20 % (v/v) glycerol previously to be immersed in liquid nitrogen.

Diffraction data were collected in the XALOC beamline at the ALBA synchrotron (Barcelona, Spain). The collected data were integrated and scaled with XDS [28] and merged using AIMLESS from the CCP4 suite package [29]. The structure was indexed in the $P2_1$ space group, and molecular replacement was carried out with MOLREP using the coordinates of ThChit33 from *T. harzianum* (PDB code 7ZYA) [20]. For automated rigid body refinement, REFMAC within the CCP4 suite [30] was used and 5 % of structure factor amplitudes were randomly selected

in the calculation of free R-factor. Then, COOT was used for manual adjustment [31] and at the later stages, water molecules were added, combined with final rounds of restrained refinement leading to the final statistics reported in Table 1.

Verification of these structures was done via PDB Validation server (validate.wwpdb.org) before coordinates and associated structure factors were deposited in the Protein Data Bank (PDB). The structural figures were prepared with PyMOL.

Structural models for the L253R and A107D/D151N/A181S/M279A MpChit35 variants were manually built by mutating these positions in the MpChit35 coordinates using COOT and optimizing the number of their potential polar interactions with the extrapolated $(GlcNAc)_4$ substrate.

Table 1
Crystallographic statistics of MpChit35.

Crystal data	MpChit35
Space group	P 2_1
Molecules/a.u.	2
Unit cell parameters	
a (Å)	60.58
b (Å)	54.85
c (Å)	97.78
β (deg)	107.72
Data collection	
Beamline	XALOC (ALBA)
Temperature (K)	100
Wavelength (Å)	0.9793
Resolution (Å)	47.26–2.55 (2.66–2.55)
Data processing	
Total reflections	123,349 (13944)
Unique reflections	20,240 (2416)
Multiplicity	6.1 (5.8)
Completeness (%)	99.5 (97.4)
Mean I/σ (I)	7.5 (4.7)
$R^{\dagger}_{merge}$ (%)	18.4 (47.4)
$R^{\dagger\dagger}_{pim}$ (%)	8.0 (21.3)
Refinement	
R_{work} / $R^{\dagger\dagger\dagger}_{free}$ (%)	18.1/23.8
N° of atoms/average B (Å^2)	
Macromolecules	4541/25.50
Ligands	75/57.02
Solvent	151/23.62
All atoms	4767/25.94
Ramachandran plot (%)	
Favoured	96.5
Outliers	0.17
RMS deviations	
Bonds (Å)	0.005
Angles (°)	1.436
PDB accession code	9HJ7

Values in brackets are for the hight-resolution shell. †Rmerge = ∑hkl ∑i | Ii(hkl) – [I(hkl)]| / ∑hkl ∑i Ii(hkl), where Ii(hkl) is the ith measurement of reflection hkl and [I(hkl)] is the weighted mean of all measurements. ††Rpim = ∑hkl [1/(N−1)] 1/2 ∑i | Ii(hkl) – [I(hkl)] | / ∑hkl ∑i Ii(hkl), where N is the redundancy for the hkl reflection. †††Rwork / Rfree = ∑hkl | Fo – Fc | / ∑hkl | Fo |, where Fc is the calculated and Fo is the observed structure factor amplitude of reflection hkl for the working / free (5 %) set, respectively.

2.5. Statistical analysis

All statistical analyses were performed using GraphPad Prism software version 10.0 (GraphPad Software, Boston, Massachusetts USA). Data were first tested for normality using the Shapiro-Wilk test. When sample values did not meet the assumptions of normality, non-parametric statistical methods were applied. Thus, a Kruskal-Wallis test was used to compare the specific activity values, followed by Dunn's multiple comparisons on all mutants versus the wild-type enzyme.

3. Results and discussion

3.1. Overall folding of MpChit35

The chitinase MpChit35 from *M. pulcherrima* was produced in *K. phaffii* as previously referred [24], then the protein was deglycosylated by EndoH treatment and purified through a monoQ column prior to crystallization experiments. The crystal structure of MpChit35 was determined at a resolution of 2.55 Å (Fig. 1A). The experimental details and methods used for structural determination are outlined in the Materials and Methods section and in Table 1. The crystals belong to the $P2_1$ space group, containing two molecules per asymmetric unit and 42 %

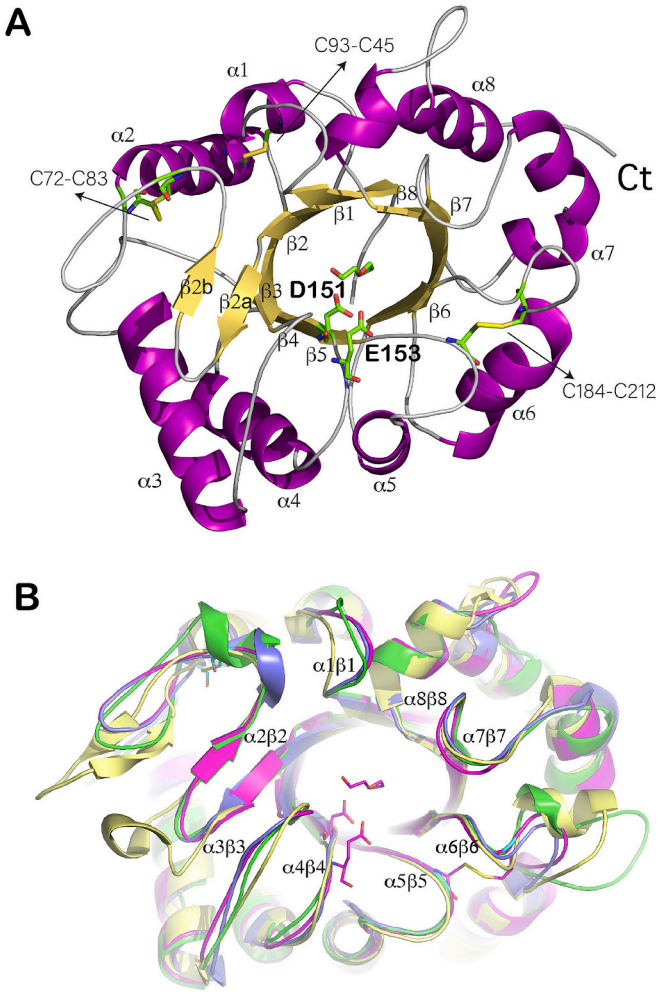

Fig. 1. MpChit35 folding. (A) MpChit35 folds into an $(\beta/\alpha)_8$-barrel typical to the GH18 family. The catalytic residues, a trapped PEG molecule, and the Cys residues making disulphide bridges are coloured as green sticks. (B) Structural superimposition of MpChit35 (violet) onto chitinase ScCTS1 from *S. cerevisiae* in blue (PDB code 2UY2), ThChit33 from *T. harzianum* (PDB code 7ZYA) in green and AfChiA1 from *A. fumigatus* in yellow (PDB code 4TX6).

solvent content within the cell. The structure was solved using molecular replacement with the coordinates of the *endo*-acting chitinase ThChit33 from *T. harzianum*, as the template [20]. The electron density maps showed the polypeptide chain from Gln21 to Asp311, the last 27 residues at the C-terminus (Val312-Val338) being invisible and probably extending from the protein core to the solvent. MpChit35 shows the structural features previously described for other GH18 chitinases, being folded into a $(\beta/\alpha)_8$-barrel domain with characteristic short α1 and bent β8, and with the presence of two β-strand insertions after β2 as a common feature among GH18 chitinases. The active site is delineated by the short loops connecting β to α motifs within the barrel, which makes a tiny cavity diverging from the bacterial-type chitinases that present large groove-shaped active-site clefts. Furthermore, three intramolecular disulphide bonds, Cys45-Cys93, Cys72-Cys83 and Cys184-Cys212, are detected in the MpChit35 polypeptide chain, which are conserved in its reported homologues from yeast and fungus. In particular, the Cys184-Cys212 bridge is linking the β5α5 to the β6α6 loop (Fig. 1A), therefore contributing to shape the positive portion of the active site cavity.

The DxDxEx conserved motif is located at the end of strand β4 within the barrel, where Glu153 is the catalytic acid protonating the glycosidic bond and Asp151 assists the acetamido group in its nucleophilic attack and stabilizes the developing positive charge on the oxazolinium ion. A polyethylene glycol (PEG) molecule from the precipitant solution was captured at the active site of the crystals, stacking against Trp281 and making polar interactions through its hydroxyl groups with the catalytic Asp151, and with Ala107 main chain, all these residues being involved in substrate binding as commented below.

A Dali search with MpChit35 coordinates reveals closest homology to fungal chitinase domain of CTS1 from *S. cerevisiae* (ScCTS1, PDB code 2UY2, RMSD 1.3 Å for 281 aligned Cα, 53 % identity) [32], followed by ThChit33 from *T. harzianum* (ThChit33, PDB code 7ZYA, RMSD 1.6 Å for 277 aligned Cα, 40 % identity) [20], ChiA1 from *Aspergillus fumigatus* (AfChiA1, PDB code 4TX6, RMSD 1.6 Å for 278 aligned Cα, 38 % identity) [33] and the model plant chitinase hevamine from *Hevea brasiliensis* (PDB code 1HVQ, RMSD 1.7 Å for 261 aligned Cα, 35 % identity) [34].

As shown in Fig. 1B, and except for β1α1, the length and conformation of the loops surrounding the active site of MpChit35 are well conserved, resulting in all proteins having similar small pocket-like, solvent-exposed substrate-binding grooves. Therefore, the differences in specificity and selectivity observed among them [20,24] are attributed to the composition of the residues located within the cavity in each case (Fig. 2).

3.2. Substrate binding mode

To go deeper into the active site specificity and selectivity, and identify the relevant residues regulating activity, some attempts to crystallize an inactivated MpChit35 variant with its $(GlcNAc)_4$ substrate were performed. As the native crystals presented its active site cavity blocked by loops from the adjacent symmetry-related molecules, new co-crystallization trials of the inactive MpChit35-D151A/E153A double mutant with the substrate were accomplished to look for different crystal forms, but all the efforts were unsuccessful. Therefore, we have modelled the $(GlcNAc)_4$ molecule within the active site cavity by structural superimposition of the reported complex with $(GlcNAc)_4$ of the ThChit33-D165A/E167A mutant homologue [20] onto the coordinates of wild-type MpChit35. As shown in Fig. 3A, the distorted conformation of the substrate at the cleavage site experimentally observed fits well within the MpChit35 active site cavity, and, therefore, the model complex may elucidate the key features controlling its binding. Fig. 3B shows how $(GlcNAc)_4$ binds tightly at subsites −2 to +2 through many hydrogen links to several residues. In addition, and as seen previously in other chitinase complexes, there may be additional water molecules contributing to fix the substrate, but the above-mentioned occupancy of the active site by adjacent molecules in the crystal, together with the trapped PEG, prevents observation of these putative water molecules.

At subsite −2, the CO from the *N*-acetyl moiety is fixed by direct hydrogen bonds to the side chain of Ser34, in its double conformation, and to Trp281 (Fig. 3B). Additionally, O6 from the sugar makes hydrogen link to Ser108, both directly and through a water molecule. These interactions are conserved in the reported ThChit33-$(GlcNAc)_4$ complex, which also presents additional links to the protein through many ordered water molecules [20].

At subsite −1, the distorted boat conformation that was firstly trapped in the ThChit33-$(GlcNAc)_4$ complex crystal presents a conserved binding mode with that reported, i.e., the sugar ring is stacked to Trp281, while its O3 is making hydrogen bond to the Ala107 main-chain, and the O6 is hydrogen linked to Asn209 side-chain and to the Ser250 main-chain. Similarly, it is expected that the *N*-acetyl group may be linked through a putative unobserved water molecule to the conserved residues Gln206 and Tyr208, this Tyr being necessary to trigger the productive positioning of the *N*-acetyl moiety for its nucleophilic attack to C1 allowing efficient catalysis.

At the positive portion of the active site, in subsite +1 (Fig. 3B), O6 is tightly fixed by three hydrogen bonds to the side-chains of Gln183, Gln206 and Asn209. These interactions seem essential in stabilizing the precise bent conformation of the bound substrate, as Asn209 is clamping the rings at the −1 and +1 subsites, while Gln183 is connecting the sugars bound to subsites +1 and +2. These three residues are conserved in the MpChit35 homologues from yeast and fungus (Fig. 2) and, therefore, may constitute a general trait in these plant-type chitinases. At subsite +2, the *N*-acetyl group is further bound to the Asn210 side-chain.

Additional binding subsites at the aglycon are not expected, as the modelled $(GlcNAc)_4$ points to the solvent. On the contrary, MpChit35 might be able to allocate additional GlcNAc units at its negative part of the cavity as is disclosed in Fig. 3C, showing a superimposition of MpChit35 with the reported hevamine-$(GlcNAc)_4$ complex [36] that includes the substrate occupying subsite −4 to −1. In particular, the protruding side-chain of Trp73 may shape a putative −5 subsite that could constitute an extended platform for binding GlcNAc units distal from the cleavage site. This Trp is not a conserved position among other chitinases and possibly accounts for the marked activity observed in the polymeric chitin, despite MpChit35 apparently being an *exo*-chitinase [24].

In summary, the active site of MpChit35 is a shallow cavity presenting Trp281 as the only aromatic residue constituting the hydrophobic platform, a feature shared with its plant-type homologues. In general, each sugar would make two hydrogen links one through the acetyl and the other through the O3/O6 hydroxyls, with the exception the GlcNAc bound at subsite +1 that presents its *N*-acetyl group pointing to the solvent. At the negative portion of the active site, subsites −2 and − 1 are delineated by short side-chain residues from loops β1α1 (Ser34), β3α3 (Ala107, Ser108) and the end of loop β7α7 (S250), a trait shared by its homologues except in ThChit33, where the equivalent to Ala107 is Asp117, and AfChiA1, with its bulky Tyr125 being equivalent to the MpChit35 Ser108 (Fig. 2). Similarly, at the positive portion, loops β5α5 (Gln183) and β6α6 (Gln206, Asn209, Asn210) stabilize the bound substrate through hydrogen links to very conserved polar residues. However, lack of prominent long residues at the β7α7 loop, (Gly252, Leu253) impedes additional polar links to the *N*-acetyl group at subsite +1, as it has been observed in the ThChi33-$(GlcNAc)_4$ complex, where the long-chain of Arg274 also stabilizes the +1/+2 glycoside bond. Finally, additional putative binding subsites at the distal negative portion are shaped mostly by the long β2α2 loop, which is variable in length and composition among the homologues chitinases (Fig. 2).

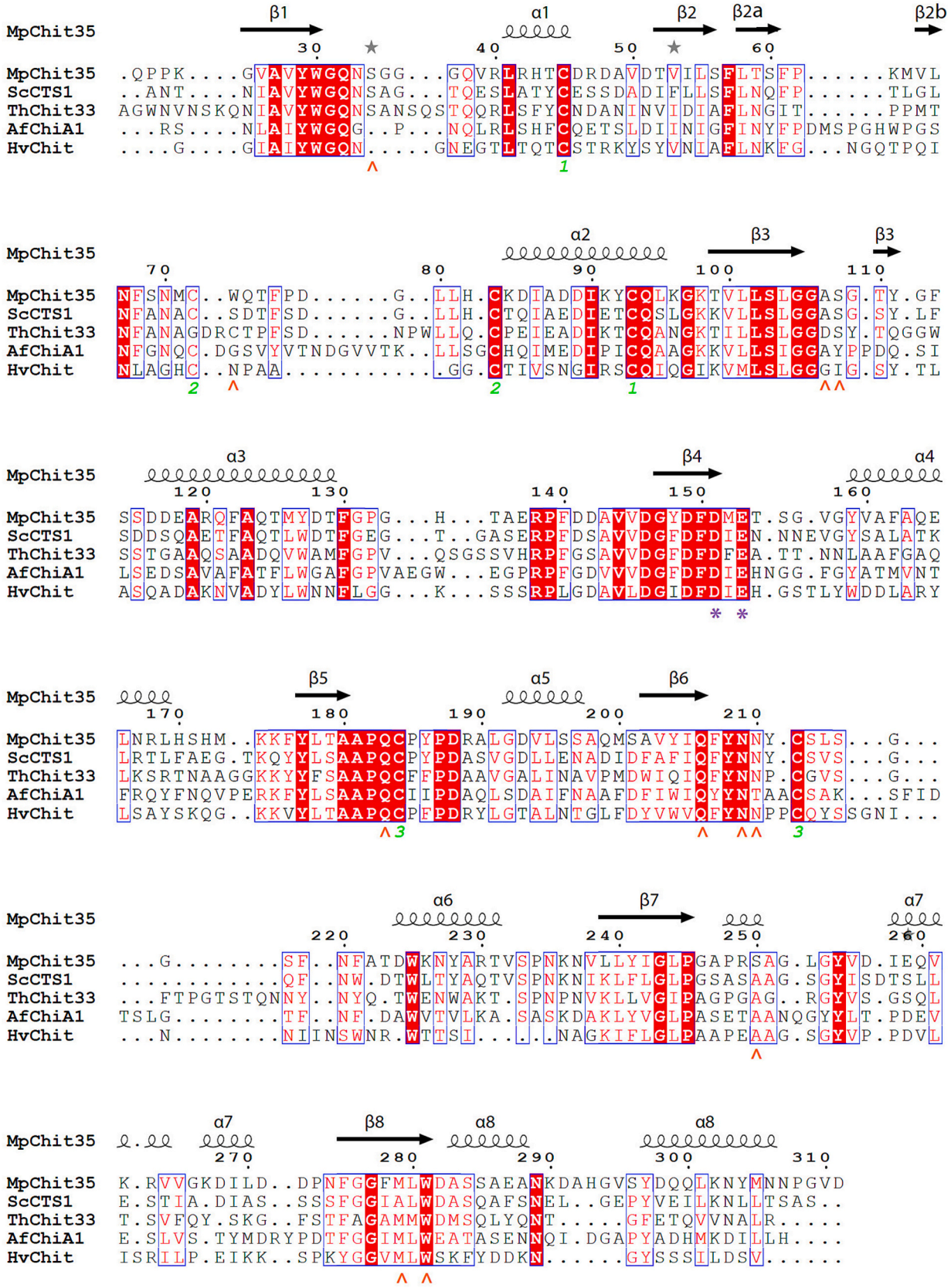

Fig. 2. Structural alignment of MpChit35 with the closet homologues. Asp151 and Glu153 in MpChit35 from the DxDxEx conserved motif are highlighted with purple asterisks. The relevant residues defining the positive and negative portions of the active site are shown with orange triangles and the cysteine residues (Cys45-Cys93, Cys72-Cys83 and Cys184-Cys212) constituting the intramolecular disulphide bridges, in green numbers. Sequences belong to MpChit35 (PDB 9HJ7), CTS1 from *S. cerevisiae* (ScCTS1, PDB 2UY2), ThChit33 from *T. harzianum* (ThChit33, PDB 7ZYA), ChitA1 from *A. fumigatus* (AfChiA1, PDB 4TX6) and plant chitinase from *H. brasiliensis* (HvChit, PDB 1HVQ); (ESPript 3.0 - https://espript.ibcp.fr). Alignment done by Dali [35].

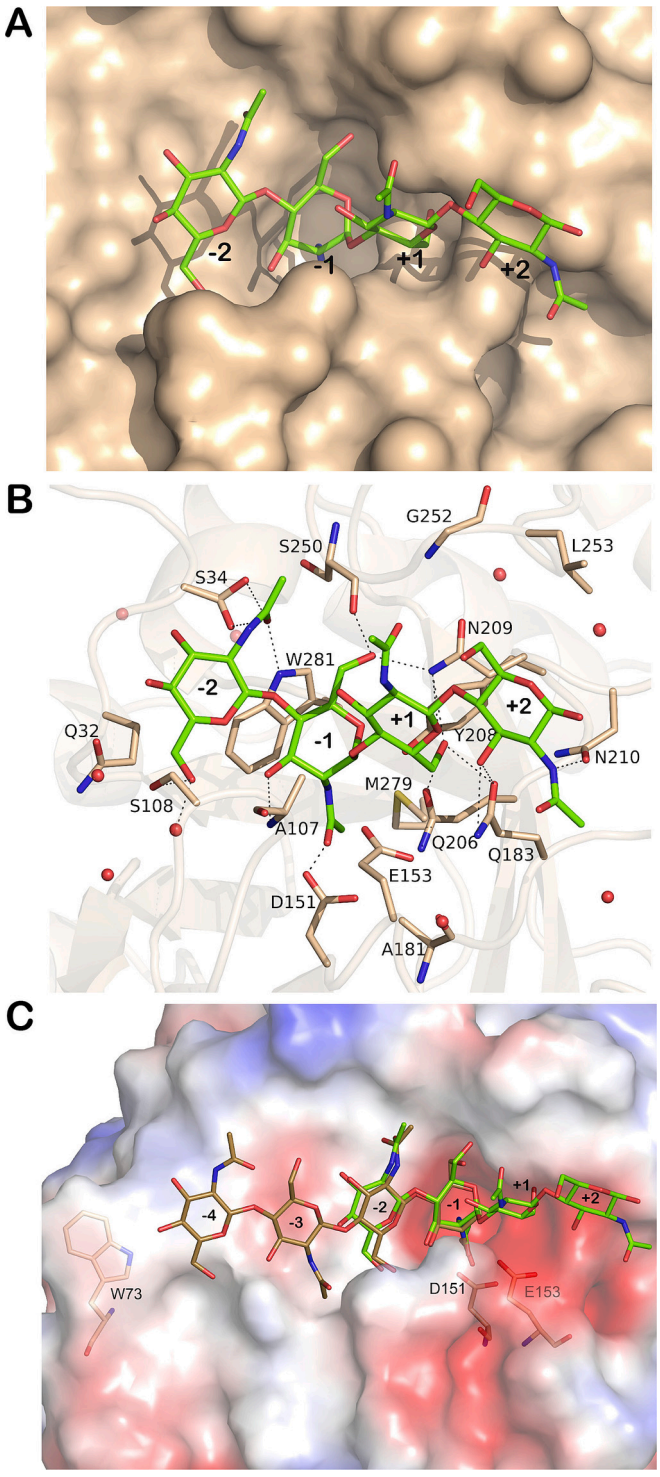

Fig. 3. The MpChit35 active site showing the proposed binding of a COS chain. Sugar was modelled into the active site by structural superimposition with the reported complex of the *T. harzianum* ThChit33-D165A/E167A mutant homologue with $(GlcNAc)_4$ (PDB code 7ZY9). (A) Molecular surface of MpChit35, showing the sugar in green sticks. (B) Details of the atomic interaction between $(GlcNAc)_4$ and MpChit35 relevant residues represented in wheat sticks, with proposed hydrogen links represented as dashed lines. (C) Molecular surface of MpChit35 and charge distribution, with positive regions coloured in blue and negative regions in red. The modelled $(GlcNAc)_4$ is represented in green sticks. A second $(GlcNAc)_4$ chain at the negative portion of the active site is extrapolated by structural superimposition of MpChit35 with the reported hevamine-$(GlcNAc)_4$ complex (PDB code 1KR1).

3.3. Substrate splitting mode

As previously mentioned, despite their high sequence (Fig. S1) and structural homology, MpChit35 and MpChit38 exhibit distinct catalytic behaviours. MpChit35 acts as an *exo*-chitinase, producing $(GlcNAc)_2$ from colloidal chitin, while MpChit38 functions as an *endo*-chitinase, generating $(GlcNAc)_3$ as the main final product [24]. To clarify their bond-splitting modes, we analysed the products formed from fully acetylated COS (*fa*COS) as substrates. Both enzymes hydrolysed $(GlcNAc)_4$ and $(GlcNAc)_6$ (Fig. 4), but neither could degrade $(GlcNAc)_2$ or $(GlcNAc)_3$, even after 24 h. This confirms that a minimum of four GlcNAc units is required for substrate hydrolysis, consistent with previous observations from CC hydrolysis [24].

MpChit35 and MpChit38 produced $(GlcNAc)_2$ and $(GlcNAc)_3$ from $(GlcNAc)_4$, while $(GlcNAc)_2$, $(GlcNAc)_3$, and $(GlcNAc)_4$ were generated from $(GlcNAc)_6$, though in different proportions. MpChit35 rapidly cleaved $(GlcNAc)_6$ into $(GlcNAc)_2$ + $(GlcNAc)_4$ but also occasionally acted at the central glycosidic bond, yielding minor amounts of $(GlcNAc)_3$ (Fig. 4A). Interestingly, in the early reaction stages, similar amounts of $(GlcNAc)_2$ and $(GlcNAc)_4$ were detected, differing from the *exo*-processive chitinases SmChiA and SmChiB [19]. However, after only 2 h, $(GlcNAc)_6$ was completely degraded, with $(GlcNAc)_2$ as the main final product. Conversely, MpChit38 exhibited lower efficiency in degrading $(GlcNAc)_6$, generating similar amounts of $(GlcNAc)_2$, $(GlcNAc)_3$, and $(GlcNAc)_4$ (Fig. 4B). Notably, just after a 15 min, 19 % of $(GlcNAc)_6$ was converted to $(GlcNAc)_3$ by MpChit35, whereas MpChit38 converted 44 %, supporting its classification as a typical plant-type *endo*-chitinase, and their differences in selectivity. These results align with previous data from CC hydrolysis [24] and are consistent with findings on MfChi from *Metschnikowia fructicola*, which shares 98.3 % sequence identity with MpChit38 and exhibits endo-chitinase activity when hydrolysing 4-nitrophenyl-β-D-N,N′,N″-tri-acetyl-chitotriose [37].

The differences between MpChit35 and MpChit38 can be attributed not only to their cleavage preferences but also to their processing rates. MpChit38 exhibited lower specificity for $(GlcNAc)_4$ compared to MpChit35 (Fig. 4C, 4D). Additionally, in both enzymes, hydrolysis rates increased with substrate polymerization degree, as longer chitin oligomers were processed more efficiently.

3.4. Mutagenic analysis to locate positions involved in the hydrolytic activity

Undoubtedly the structural analysis of the MpChit35-$(GlcNAc)_4$ complex provides a solid basis for identifying residues that can be substituted to alter its enzymatic activity, but also the comparison of the protein sequence with that of its homologues can position some key residues for activity (Fig. 2). Initially the MpChit35 catalytic Asp151/Glu153 were changed to Ala or Asn to attempt crystallization of the enzyme-substrate complex. According to the observed enzyme-substrate atomic interactions, at the negative portion of the active site, subsites −2 (Fig. 3B), Ala107 and Ser108 (loop β3α3) were substituted by Asp and Tyr, respectively, also the equivalent residues in ThChit33 and AfChiA1. The A107W change was also tried, in an attempt to introduce an aromatic residue in this position that could potentiate the substrate binding at −2 subsite enhancing hydrolytic activity. In addition, the role of Trp73 in binding chitin was also investigated through the W73D change to alter the proposed putative distal subsite (Fig. 3C). With respect to the positive portion of the active site, several polar residues were introduced at G252/L253 positions (loop β7α7), to increase the interaction of the substrate with the protein at subsites +1/+2. Finally, two variable positions next to the catalytic *N*-acetyl group at subsite −1 were investigated, Ala181 (loop β5α5) and Met279 (strand β8), which were changed to Ser and Ala, respectively, residues found in other close MpChit35 homologues (Fig. 2), and in MpChit38 from *M. pulcherrima* [24] (Fig. S1).

Site-directed mutagenesis was used to introduce the missense

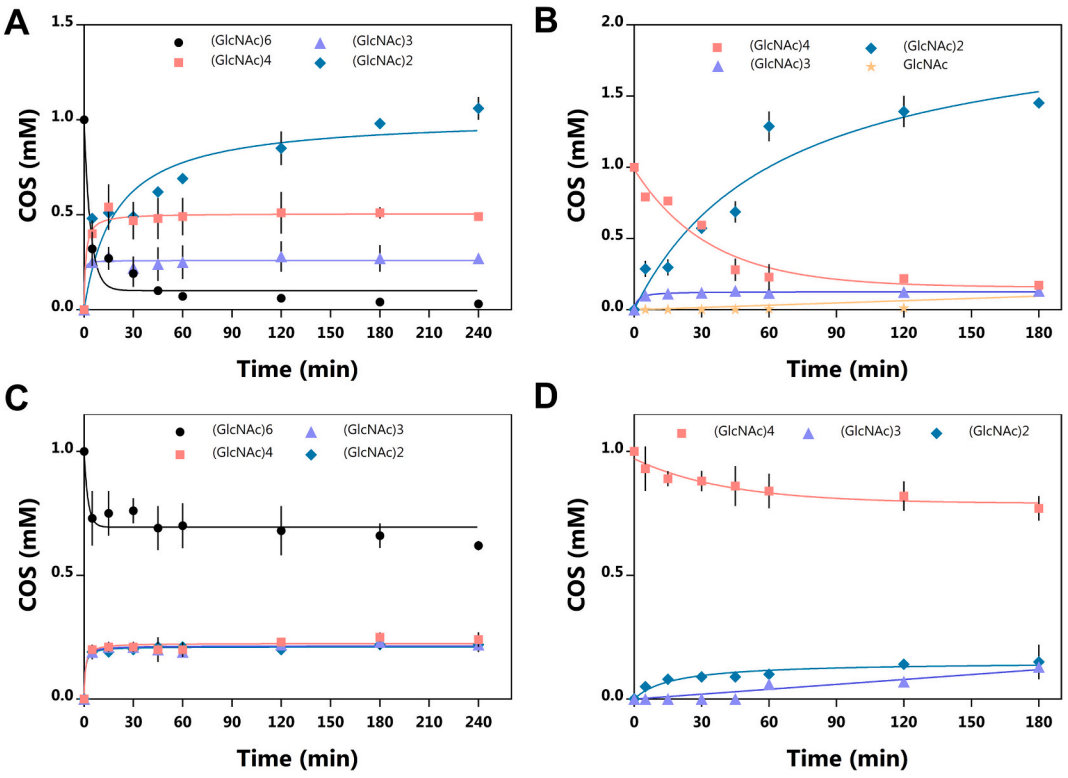

Fig. 4. Time-course degradation of $(GlcNAc)_6$ and $(GlcNAc)_4$ by MpChit35 and MpChit38. Hydrolysis of $(GlcNAc)_6$ (A) and $(GlcNAc)_4$ (B) by MpChit35. Hydrolysis of $(GlcNAc)_6$ (C) and $(GlcNAc)_4$ (D) by MpChit38. Data were obtained by HPLC-ELSD analysis. All reactions were performed in duplicate, and standard errors are indicated. Reactions were carried out at the same enzyme concentration (20 nM) to assess substrate cleavage patterns and product distribution.

mutations W73D, A107D/W, S108Y, D151A/N, E153A, A181S, G252D/S, L253R/Q, and M279A. This was done using specifically designed pairs of primers (Table S1) and the previously reported pIB4-MpChit35 construct [24]. The resulting MpChit35 variants were then produced in *K. phaffii* cultures, and their hydrolytic activities were assessed on CC. Most of them displayed a slight drop in activity on this substrate (W73D, A107D, S108Y, G252S, G252D) (Fig. 5). As expected, the substitutions at the catalytic residues Asp151 and Glu153 led to a drastic reduction in specific activity. Moreover, introducing a bulky Trp side chain at position 107 and removing the Met279 side-chain from the positive part of the catalytic cavity significantly hampered the hydrolytic ability. Consequently, kinetic assays of all those MpChit35 variants (Table 2, Fig. S2) revealed that their apparent catalytic efficiency (k_{cat}/K_m) on CC was reduced compared to that of the wild-type enzyme. The kinetic parameters for A107W, D151A, and E153A could not be determined due to their very low activities (Fig. 5). Although the apparent affinities (K_m values) of the A107D, S108Y, and G252S/D variants were slightly higher, their k_{cat} values were also significantly lower than those of the wild-type MpChit35 protein, leading to the detected drop in their catalytic efficiency. In contrast, the marked loss in apparent affinity (K_m values increased by about 3-fold) for W73D may trigger the change in its

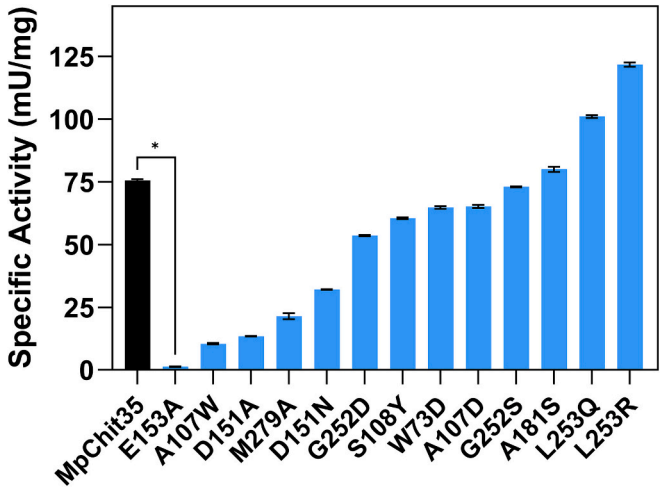

Fig. 5. Hydrolytic activity on colloidal chitin of MpChit35 variants. Specific activity data (mU/mg of protein) are the average of three independent experiments, and standard errors are indicated. Colloidal chitin (10 mg/mL) was used as substrate. Asterisks indicate statistically significant differences compared to the wild-type enzyme ($p < 0.05$; $n = 3$).

Table 2
Apparent kinetic parameters of MpChit35 variants on colloidal chitin.

Variant	K_m ($\mu g \cdot \mu L^{-1}$)	k_{cat} (s^{-1})	k_{cat}/K_m ($s^{-1} \cdot \mu L \cdot \mu g^{-1}$)
MpChit35	25 ± 5	1.5 ± 0.10	0.06 ± 0.01
W73D	64 ± 10	1.7 ± 0.10	0.03 ± 0.01
A107D	4.9 ± 0.9	0.1 ± 0.01	0.03 ± 0.01
S108Y	13 ± 3.1	0.3 ± 0.02	0.02 ± 0.01
D151N	2.1 ± 0.4	0.1 ± 0.04	0.02 ± 0.01
A181S	1.0 ± 0.1	0.1 ± 0.01	0.08 ± 0.02
G252D	5.8 ± 0.9	0.3 ± 0.02	0.05 ± 0.01
G252S	17 ± 3.7	0.7 ± 0.07	0.04 ± 0.01
L253R	2.7 ± 0.4	0.4 ± 0.02	0.17 ± 0.02
L253Q	3.9 ± 0.7	0.3 ± 0.02	0.10 ± 0.01
M279A	36 ± 9.8	0.8 ± 0.07	0.02 ± 0.01
D151N/A107D/A181S/M279A	0.5 ± 0.1	0.1 ± 0.01	0.05 ± 0.01
A107D/L253R	17 ± 4	1.8 ± 0.2	0.10 ± 0.06

Reaction velocity measurements were performed in triplicate and standard errors are indicated. k_{cat} values calculated from V_{max} considering the molecular weights in Da for each protein variant. V_{max} refers to the maximum rate of reaction, in micromoles of reducing sugars released per min.

catalytic efficiency, supporting the hypothesis that the non-conserved Trp73 residue could be involved in substrate binding by contributing to distal interactions with the polymer chains, and conforming an additional −5 subsite. In fact, accumulating evidence has shown that tryptophan-mediated interactions with the chitinous substrates are key determinants of enzyme processivity and its directionality in well-studied processive bacterial-type *exo*-acting chitinases like SmChiA, SmChiB and ThChit42 [4,16,18]. Moreover, the bacterial-type non-processive mammalian *endo*-chitinase HCHT also contains numerous Trp residues, which likely mediate interactions that help overcome the substrate decrystallization penalty associated with their *endo*-binding type [4]. Although MpChit35 lacks the abundance of aromatic residues that characterise the aforementioned enzymes, the W73D variant highlights the crucial importance of aromatic residue-mediated enzyme-substrate interactions near the catalytic centre and suggests a connection between the substrate-binding mechanisms of bacterial-type chitinases and those of plant-type chitinases. On the other hand, the specific activities of the A181S and L253Q/R variants (Fig. 5) were boosted. In fact, they showed about a 2-fold increase (A181S and L253Q) and a 3-fold increase (L253R) in their apparent catalytic efficiency, mainly due to their higher affinities (lower K_m values) for the substrate (Table 2, Fig. S1), potentially by the establishment of crucial polar interactions at −1 (A181S) and, most importantly, at +2 (L253R/Q) subsites, as it will be seen below. These preliminary results highlight the crucial role of polar interactions in the +2 subsite for designing biocatalysts with enhanced catalytic efficiency. A similar behaviour was observed in the chitinase ThChit33, where the mutation of Arg274 (homologous to Leu253 in MpChit35) to Ser, a less polar amino acid, led to a reduction in catalytic efficiency when using CC as a substrate [20].

3.5. Altering the COS splitting mode

The MpChit35 positions Ala107, Asp151, Ala181, and Met279 are not conserved in the homologue MpChit38 chitinase, with which it shares 78.3 % sequence homology. Instead, in MpChit38 these positions are occupied by Asp107, Asn151, Ser181, and Ala279, respectively (Fig. S1). The MpChit35 variants A107D, D151N, A181S, and M279A as well as the multiple mutant variant containing all the referred single-point mutations (A107D/D151N/A181S/M279A) were obtained, and their activities against $(GlcNAc)_4$ and $(GlcNAc)_6$ were analysed by HPLC-ELSD (Figs. 6 and S3, S4, S5), along with that of the L253R variant, which showed the greatest apparent catalytic efficiency on CC (Table 2). Thus, the molar ratio of $(GlcNAc)_3$ to $(GlcNAc)_2$, which reflects the preference of the enzymes for producing trimers versus dimers at specific times of the reaction were evaluated (Fig. 6A, 6B). Moreover, we determined the final yield of products formed from the $(GlcNAc)_6$ and $(GlcNAc)_4$ hydrolytic reactions (Fig. S5).

Notably, the A107D/D151N/A181S/M279A variant (referred to as multiple variant) exhibited a significant increase in $(GlcNAc)_3$ production from $(GlcNAc)_6$ during all the analysed reaction times. A very similar cutting pattern to that obtained with MpChit38 (Fig. 6A), as higher trimers/dimers ratios were detected in the multiple variant compared to MpChit35 wild-type, indicating its stronger preference for producing trimers. This change in selectivity was also detected when using $(GlcNAc)_4$ as substrate (Fig. 6B), supporting the idea that the substituted residues play a crucial role in the *endo*-activity of the wild-

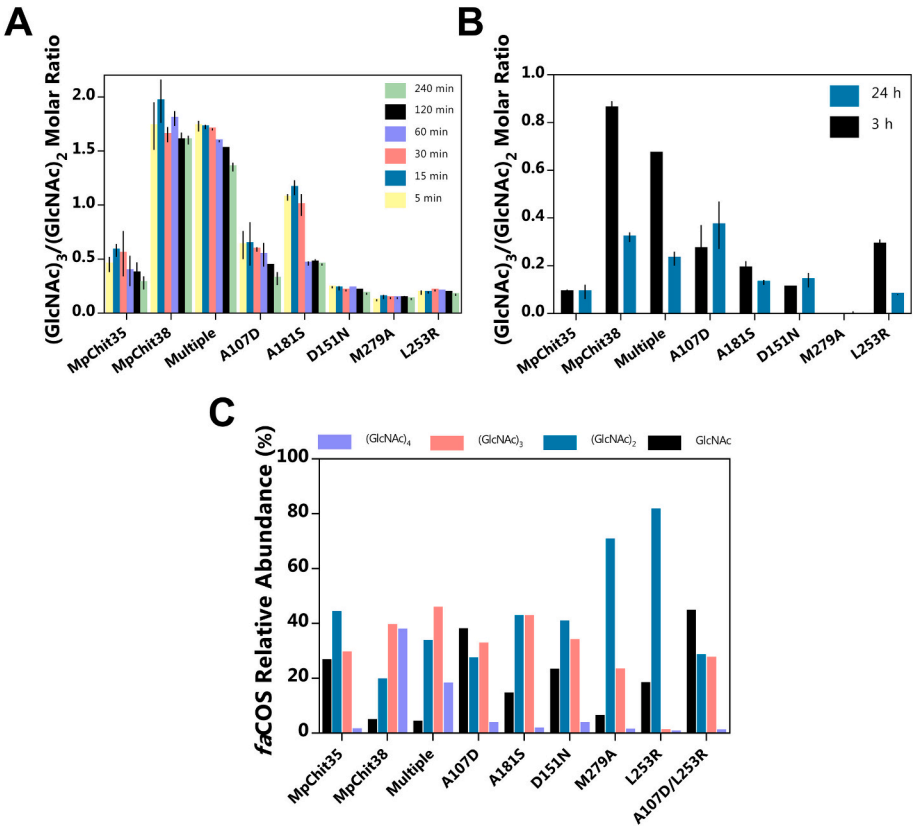

Fig. 6. Impact of relevant mutations in the cleavage mode. (A) Ratio of $(GlcNAc)_3$ to $(GlcNAc)_2$ resulting from the hydrolysis of $(GlcNAc)_6$ at the referred reaction times. (B) Ratio of $(GlcNAc)_3$ to $(GlcNAc)_2$ resulting from the hydrolysis of $(GlcNAc)_4$ after 3 and 24 h. The molar ratio was determined based on the measured concentrations of the trimer and dimer products at the specified reaction times by HPLC-ELSD analysis. All reactions were performed in duplicate, and standard errors are indicated. Statistical differences were evaluated using the Kruskal-Wallis test followed by Dunn's multiple comparisons versus the wild-type and no individual comparisons reached significance after correction. (C) COS profiles formed when using colloidal chitin as substrate, analysed by MALDI-TOF mass spectrometry. The relative abundance of each product was calculated based on the total intensities of the *fa*COS formed. Detailed intensities for each compound are provided in Table S2.

type MpChit38 enzyme. Specifically, A107D and A181S appear to be crucial variants responsible for the differences in the splitting mode, as the final yield of $(GlcNAc)_3$ from $(GlcNAc)_4$ and $(GlcNAc)_6$ was higher compared to that of the MpChit35 enzyme (Fig. 6A, 6B). This preference is also reflected in the final COS yield (Fig. S5). In contrast, substitutions D151N and, notably, M279A enhance the release of dimers from the $(GlcNAc)_6$. Similarly to what happens with the variant including the change M279A, that including L253R also improves the release of dimers from both substrates (Fig. 6A, 6B).

To further analyse the splitting mode preferences of these variants, we also examined the product composition of reaction mixtures when using CC as substrate by MALDI-TOF mass spectrometry (Fig. 6C, Table S2). This analysis also included the MpChit35 variants containing substitutions G252D, W73D, and S108Y, along with a double mutant that combines the A107D and L253R mutations (A107D/L253R). The kinetic parameters of this double mutant were previously evaluated (Table 2), revealing enhanced affinity for colloidal chitin, as evidenced by lower K_m values, along with an increased k_{cat}, both contributing to improved overall catalytic efficiency. The MpChit35 variants including the W73D, D151N and G252D mutations showed similar product profiles to the wild-type MpChit35 (Table S2), but a notable shift toward dimer production was detected, particularly when the enzyme includes the M279A and L253R changes, the latter of which completely lost trisaccharide production, indicating an enhanced *exo*-acting activity (Fig. 6C, Table S2). These findings align with our previous results from COS hydrolysis reactions (Fig. 6A, 6B).

Interestingly, the multiple mutant of MpChit35 produced a profile of COS comparable to the wild-type MpChit38, with improved *endo*-acting activity reflected by increased trimer production and remarkable tetramer intensities. The mutation A181S also favoured trimers production, though tetramer production was reduced (Fig. 6C), likely due to its higher substrate specificity compared to that of MpChit38 (Fig. 4, Fig. S4C). The mutation S108Y primarily generated monosaccharides (Table S2), while the A107D, though also monosaccharide-biased, produced significant levels of dimers and trimers (Fig. 6C, Table S2). In fact, the A107D variant required only 5 nM of enzyme for cleaving $(GlcNAc)_4$ (Fig. S3B), demonstrating its far greater specificity compared to the 100 nM required by the wild-type variants of MpChit35 and MpChit38 to hydrolyse this substrate (Fig. 4B, 4D).

Moreover, the product profile of the variant including mutations A107D/L253R closely resembled that of the variant including the A107D single mutation rather than the L253R one (Fig. 6C), suggesting that the Asp residue at the −1 subsite plays a crucial role in determining the specificity of the plant-type chitinases. As we previously referred, the homologous residue Asp117 in ThChit33 was demonstrated to fix the distorted conformation of the substrate at −1 subsite and to clamp the bended of its conformation [20]. This residue is non-conserved between members of the plant-type GH18 chitinase (Fig. 2). Thus, the findings found in this study confirm and suggest that an Asp located at this position, at the end of the conserved GH18 sequence SxGGx, plays a crucial role in modulating the specificity and cleavage patterns of plant-type chitinases.

From a structural perspective, the L253R mutation, which leads to a threefold increase in catalytic activity (Table 2), is predicted to introduce new polar interactions with the substrate at the positive subsites of MpChit35. Structural modeling of the variant (Fig. 7A) suggests that the arginine side chain may interact specifically with the O6 hydroxyl group of the GlcNAc residue at the +2 subsite. The substitution of Leu253, a nonpolar residue, with a positively charged, polar arginine likely enhances substrate binding affinity and promotes enzyme processivity, thereby increasing catalytic efficiency and promoting *exo*-activity. These findings support growing structural evidence indicating that polar residues at the positive subsites, in addition to aromatic ones, are critical modulators of substrate engagement and processive catalysis. For instance, mutating the polar residue Thr276 to alanine in the processive binding cleft of bacterial-type SmChiA from *Serratia marcescens* resulted

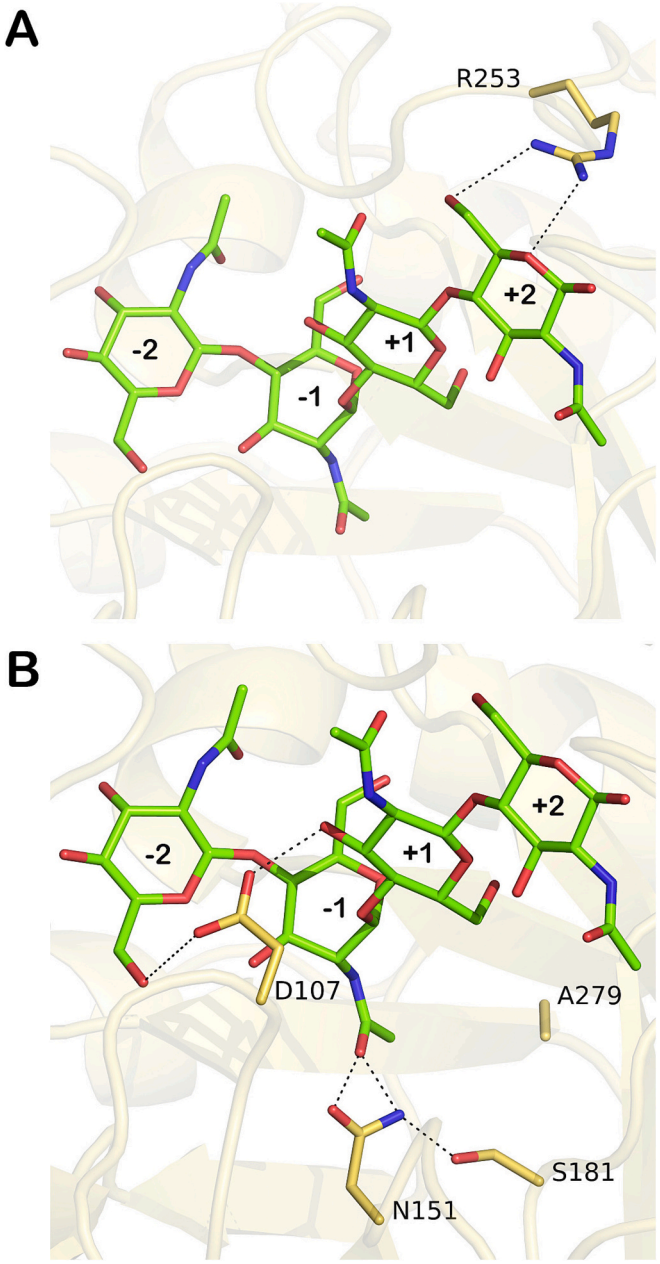

Fig. 7. Models for relevant MpChit35 variants modifying its activity on chitin. Proposed structures of the MpChit35 variants including substitutions (A) L253R and (B) A107D/D151N/A181S/M279A, and suggested new polar interactions, represented as dashed lines, with a putative $(GlcNAc)_4$ chain extrapolated as in Fig. 3.

in reduced binding affinity and apparent processivity [38]. Similarly, substituting other polar residues, Arg294 at the +1 subsite and Glu221 at the +3 subsite, with alanine in SmChiB from *S. marcescens* affected both apparent processivity, likely due to destabilization of stacking interactions involving key aromatic residues in the cleft, and ligand binding [39]. While those examples refer to bacterial *exo*-chitinases, our findings reveal that similar principles also apply to MpChit35, a yeast GH18 enzyme structurally related to *endo*-chitinases, highlighting the broader relevance of polar contacts at positive subsites for enhancing binding and processivity.

Conversely, the A181S substitution is predicted to allow the serine side chain to form a hydrogen bond with Asn151, potentially enhancing the role of Asn151 in stabilizing the charge of the reaction intermediate. This mutation is part of the A107D/D151N/A181S/M279A multiple

mutant, whose modelled structure is shown in Fig. 7B. Remarkably, this variant exhibits a cleavage profile comparable to MpChit38, characterised by a shift toward increased endo-acting activity, despite the presence of D151N and M279A, which individually promote dimer release. These observations suggest that A107D and A181S play a predominant role in determining the substrate cleavage mode of the multiple mutant (Fig. 6).

4. Conclusions

This study presents a detailed structure-function analysis of the MpChit35 chitinase from the yeast *Metschnikowia pulcherrima*, revealing its characteristic open, solvent-exposed active site typical of plant-type chitinases, in contrast to its bacterial counterparts. This structure is characterised by predominantly short residues, except in the positive subsites, where conserved residues such as Gln183, Gln206, and Asn209 are shared across homologues. Remarkably, the introduction of long-chain polar residues in variants such as L253R and A181S significantly enhanced catalytic efficiency. Functional analysis of MpChit35 variants (A107D, D151N, A181S, L253R, and M279A) showed substantial shifts in cleavage patterns, particularly in the release of $(GlcNAc)_2$ and $(GlcNAc)_3$. Specifically, L253R and M279A promoted processive cleavage into dimers, while A107D and A181S increased trimer release, underscoring the role of specific residues in tuning substrate specificity and processivity. Importantly, the combination of mutations A107D, D151N, A181S, and M279A shifted the behaviour of MpChit35 toward the *endo*-acting chitinase MpChit38 without compromising activity, enabling the better production of longer chito-oligosaccharides with potential bioactivities. Notably, the L253R variant acted with high processivity and product selectivity, generating almost exclusively dimers from colloidal chitin, mimicking *exo*-chitinase activity and offering promising applications in producing fermentable sugars for high-value compounds or biofuels. While the exact molecular mechanisms underlying these functional changes remain to be fully elucidated, our findings demonstrate the potential of rational enzyme engineering to fine-tune chitinase specificity, processivity, and product outcomes. Altogether, this study provides a valuable framework for engineering chitinases with for the tailored enzymatic production of specific COS, paving the way for their practical deployment in industrial biotechnology and sustainable biomass valorisation.

Accession codes

Atomic coordinates and structure factors of MpChit35 have been deposited in the Protein Data Bank (PDB), under PDB ID 9HJ7.

CRediT authorship contribution statement

Marina Minguet-Lobato: Writing – review & editing, Writing – original draft, Visualization, Software, Methodology, Investigation, Formal analysis, Conceptualization. **Ángela Fernández-García:** Methodology, Investigation. **Elena Jiménez-Ortega:** Methodology, Investigation. **Fadia V. Cervantes:** Methodology. **Pilar Sánchez-Pozo:** Investigation. **Francisco J. Plou:** Writing – review & editing, Supervision, Resources, Funding acquisition. **Julia Sanz-Aparicio:** Writing – review & editing, Writing – original draft, Resources, Funding acquisition, Formal analysis, Conceptualization. **María Fernández-Lobato:** Writing – review & editing, Writing – original draft, Supervision, Resources, Project administration, Funding acquisition, Conceptualization.

Declaration of competing interest

The authors declare that they have no known competing financial interests or personal relationships that could have appeared to influence the work reported in this paper.

Acknowledgements

This work was supported by: (1) Project GLYCOENZ-GREEN (PID2022-136367OB-C31/C32/C33), funded by MCIN/AEI/10.13039/501100011033 and FEDER, a Way of Making Europe; (2) Project SUST_CHIT_BIOPR (TED2021-129288B-C21/22) funded by MCIN/AEI/10.13039/501100011033 and by the European Union Next Generation EU/PRTR. We thank the Synchrotron Radiation Source at ALBA (Barcelona, Spain) for assistance with the BL13-XALOC beamline and to the Foundation Ramon Areces for an institutional grant to CBM. The first author was supported by grant PRE2020-092330 from the Spanish Ministry of Science and Innovation.

Appendix A. Supplementary data

Supplementary data to this article can be found online at https://doi.org/10.1016/j.ijbiomac.2025.146538.

Data availability

Data will be made available on request.

References

[1] M. Rinaudo, Chitin and chitosan: properties and applications, Prog. Polym. Sci. 31 (7) (2006) 603–632, https://doi.org/10.1016/j.progpolymsci.2006.06.001.
[2] H. Amiri, M. Aghbashlo, M. Sharma, J. Gaffey, L. Manning, S.M. Moosavi Basri, J. F. Kennedy, V.K. Gupta, M. Tabatabaei, Chitin and chitosan derived from crustacean waste valorization streams can support food systems and the UN sustainable development goals, Nat. Food 3 (10) (2022) 822–828, https://doi.org/10.1038/s43016-022-00591-y.
[3] W. Chen, X. Jiang, Q. Yang, Glycoside hydrolase family 18 chitinases: the known and the unknown, Biotechnol. Adv. 43 (2020) 107553, https://doi.org/10.1016/j.biotechadv.2020.107553.
[4] M. Sørlie, S.J. Horn, G. Vaaje-Kolstad, V.G.H. Eijsink, Using chitosan to understand chitinases and the role of processivity in the degradation of recalcitrant polysaccharides, React. Funct. Polym. 148 (2020) 104488.
[5] R. Zhang, Q. Zhao, Z. Yi, K. Zhang, J. Shi, L. Zhu, Y. Chen, J. Jin, L. Zhao, Chitin oligosaccharides for the food industry: production and applications, Syst. Microbiol. Biomanufacturing 3 (1) (2023) 49–74, https://doi.org/10.1007/s43393-022-00127-2.
[6] E. Capecchi, E. Tomaino, D. Piccinino, P.E. Kidibule, M. Fernández-Lobato, D. Spinelli, R. Pogni, A.G. Cabado, J. Lago, R. Saladino, Nanoparticles of lignins and saccharides from fishery wastes as sustainable UV-shielding, antioxidant, and antimicrobial biofillers, Biomacromolecules 23 (8) (2022) 3154–3164, https://doi.org/10.1021/acs.biomac.2c00236.
[7] Y. Liu, H. Yang, F. Wen, L. Bao, Z. Zhao, Z. Zhong, Chitooligosaccharide-induced plant stress resistance, Carbohydr. Polym. 302 (2023) 120344, https://doi.org/10.1016/j.carbpol.2022.120344.
[8] N. Annamalai, M. Veeramuthu Rajeswari, S. Vijayalakshmi, Purification and characterization of chitinase from *Alcaligenes faecalis* AU02 by utilizing marine wastes and its antioxidant activity, Ann. Microbiol. 61 (2011) 801–807, https://doi.org/10.1007/s13213-011-0198-5.
[9] S. Roseman, X. Li, D. Comb, Conversion of Chitin Into N-Acetylglucosamine, Glucosamine and Bioethanol, WO2010123784A2, World Intellectual Property Organization (WIPO). https://patents.google.com/patent/WO2010123784A2/en, 2010.
[10] J. You, M. Zhao, S. Chen, Effect of chitooligosaccharides with a specific degree of polymerization on multiple targets in T2DM mice, Bioresour. Bioprocess. 9 (2022) 94, https://doi.org/10.1186/s40643-022-00579-3.
[11] K. Mohan, A.R. Ganesan, P.N. Ezhilarasi, K.K. Kondamareddy, D.K. Rajan, P. Sathishkumar, J. Rajarajeswaran, L. Conterno, Green and eco-friendly approaches for the extraction of chitin and chitosan: a review, Carbohydr. Polym. 287 (2022) 119349, https://doi.org/10.1016/j.carbpol.2022.119349.
[12] N. Míguez, P. Kidibule, P. Santos-Moriano, A.O. Ballesteros, M. Fernández-Lobato, F.J. Plou, Enzymatic synthesis and characterization of different families of chitooligosaccharides and their bioactive properties, Appl. Sci. 11 (7) (2021) 3212, https://doi.org/10.3390/app11073212.
[13] G.M. Mathew, D.C. Mathew, R.K. Sukumaran, R. Sindhu, C.C. Huang, P. Binod, R. Sirohi, S.H. Kim, A. Pandey, Sustainable and eco-friendly strategies for shrimp shell valorization, Environ. Pollut. 267 (2020) 115656, https://doi.org/10.1016/j.envpol.2020.115656.
[14] P.E. Kidibule, J. Costa, A. Atrei, F.J. Plou, M. Fernández-Lobato, R. Pogni, Production and characterization of chitooligosaccharides by the fungal chitinase Chit42 immobilized on magnetic nanoparticles and chitosan beads: selectivity, specificity and improved operational utility, RSC Adv. 11 (2021) 5529, https://doi.org/10.1039/d0ra10409d.
[15] G. Vaaje-Kolstad, S.J. Horn, M. Sørlie, V.G.H. Eijsink, The chitinolytic machinery of *Serratia marcescens* - a model system for enzymatic degradation of recalcitrant

polysaccharides, FEBS J. 280 (13) (2013) 3028–3049, https://doi.org/10.1111/febs.12181.
[16] E. Jiménez-Ortega, P.E. Kidibule, M. Fernández-Lobato, J. Sanz-Aparicio, Structural inspection and protein motions modelling of a fungal glycoside hydrolase family 18 chitinase by crystallography depicts a dynamic enzymatic mechanism, Comput. Struct, Biotechnol. J. 19 (2021) 5466–5478, https://doi.org/10.1016/j.csbj.2021.09.027.
[17] H. Li, L.H. Greene, Sequence and structural analysis of the chitinase insertion domain reveals two conserved motifs involved in chitin-binding, PLoS One 5 (1) (2010) e8654, https://doi.org/10.1371/journal.pone.0008654.
[18] P.E. Kidibule, P. Santos-Moriano, E. Jiménez-Ortega, M. Ramírez-Escudero, M. C. Limón, M. Remacha, et al., Use of chitin and chitosan to produce new chitooligosaccharides by chitinase Chit42: enzymatic activity and structural basis of protein specificity, Microb. Cell Factories 17 (1) (2018) 47, https://doi.org/10.1186/s12934-018-0895-x.
[19] S.J. Horn, A. Sørbotten, B. Synstad, P. Sikorski, M. Sørlie, K.M. Vårum, V.G. H. Eijsink, Endo/exo mechanism and processivity of family 18 chitinases produced by *Serratia marcescens*, FEBS J. 273 (3) (2006) 491–503, https://doi.org/10.1111/j.1742-4658.2005.05079.x.
[20] E. Jiménez-Ortega, P.E. Kidibule, M. Fernández-Lobato, J. Sanz-Aparicio, Structure-function insights into the fungal endo-chitinase Chit33 depict its mechanism on chitinous material, Int. J. Mol. Sci. 23 (14) (2022) 7599, https://doi.org/10.3390/ijms23147599.
[21] P.E. Kidibule, P. Santos-Moriano, F.J. Plou, M. Fernández-Lobato, Endo-chitinase Chit33 specificity on different chitinolytic materials allows the production of unexplored chitooligosaccharides with antioxidant activity, Biotechnol. Rep. 27 (2020) e00500, https://doi.org/10.1016/j.btre.2020.e00500.
[22] K.B. Eide, A.R. Lindbom, V.G.H. Eijsink, A.L. Norberg, M. Sørlie, Analysis of productive binding modes in the human chitotriosidase, FEBS Lett. 587 (21) (2013) 3508–3513, https://doi.org/10.1016/j.febslet.2013.09.004.
[23] C.M. Payne, J. Baban, S.J. Horn, P.H. Backe, A.S. Arvai, B. Dalhus, M. Bjørås, V.G. H. Eijsink, M. Sørlie, G. Vaaje-Kolstad, Hallmarks of processivity in glycoside hydrolases from crystallographic and computational studies of the *Serratia marcescens* chitinases, J. Biol. Chem. 287 (43) (2012) 36322–36330, https://doi.org/10.1074/jbc.m112.402149.
[24] M. Minguet-Lobato, F.V. Cervantes, N. Míguez, F.J. Plou, M. Fernández-Lobato, Chitinous material bioconversion by three new chitinases from the yeast *Metschnikowia pulcherrima*, Microb. Cell Factories 23 (2024) 31, https://doi.org/10.1186/s12934-024-02300-9.
[25] H. Liu, J.H. Naismith, An efficient one-step site-directed deletion, insertion, single and multiple-site plasmid mutagenesis protocol, BMC Biotechnol. 8 (2008) 91, https://doi.org/10.1186/1472-6750-8-91.
[26] J.L. González-Alfonso, Z. Ubiparip, E. Jiménez-Ortega, A. Poveda, C. Alonso, L. Coderch, J. Jiménez-Barbero, J. Sanz-Aparicio, A. Ballesteros, T. Desmet, F. J. Plou, Enzymatic synthesis of phloretin α-glucosides using a sucrose phosphorylase mutant and its effect on solubility, antioxidant properties and skin absorption, Adv. Synth. Catal. 363 (2021) 3079–3089, https://doi.org/10.1002/adsc.202100201.
[27] F. Guan, X. Tian, R. Zhang, Y. Zhang, N. Wu, J. Sun, H. Zhang, T. Tu, H. Luo, B. Yao, J. Tian, H. Huang, Enhancing the endo-activity of the thermophilic chitinase to yield chitooligosaccharides with high degrees of polymerization, Bioresour. Bioprocess. 11 (1) (2024) 29, https://doi.org/10.1186/s40643-024-00735-x.
[28] W. Kabsch, Xds, Acta Crystallogr. D Biol. Crystallogr. 66 (2) (2010) 125–132, https://doi.org/10.1107/S0907444909047337.
[29] P.R. Evans, G.N. Murshudov, How good are my data and what is the resolution? Acta Crystallogr. D Biol. Crystallogr. 69 (7) (2013) 1204–1214, https://doi.org/10.1107/S0907444913000061.
[30] G.N. Murshudov, P. Skubák, A.A. Lebedev, N.S. Pannu, R.A. Steiner, R.A. Nicholls, M.D. Winn, F. Long, A.A. Vagin, REFMAC5 for the refinement of macromolecular crystal structures, Acta Crystallogr. D Biol. Crystallogr. 67 (4) (2011) 355–367, https://doi.org/10.1107/S0907444911001314.
[31] P. Emsley, B. Lohkamp, W.G. Scott, K. Cowtan, Features and development of Coot, Acta Crystallogr. D Biol. Crystallogr. 66 (4) (2010) 486–501, https://doi.org/10.1107/S0907444910007493.
[32] R. Hurtado-Guerrero, D.M.F. van Aalten, Structure of *Saccharomyces cerevisiae* chitinase 1 and screening-based discovery of potent inhibitors, Chem. Biol. 14 (2007) 589–599, https://doi.org/10.1016/j.chembiol.2007.03.015.
[33] D.E.A. Lockhart, A. Schuettelkopf, D.E. Blair, D.M.F. van Aalten, Screening-based discovery of *Aspergillus fumigatus* plant-type chitinase inhibitors, FEBS Lett. 588 (2014) 3282–3290, https://doi.org/10.1016/j.febslet.2014.07.015.
[34] A.C. Terwisscha van Scheltinga, K.H. Kalk, J.J. Beintema, B.W. Dijkstra, Crystal structures of Hevamine, a plant defence protein with chitinase and lysozyme activity and its complex with an inhibitor, Structure 2 (1994) 1181–1189, https://doi.org/10.1016/S0969-2126(94)80093-7.
[35] L. Holm, Dali server: structural unification of protein families, Nucleic Acids Res. 50 (W1) (2022) W210–W215, https://doi.org/10.1093/nar/gkac387.
[36] E. Bokma, H.J. Rozeboom, M. Sibbald, B.W. Dijkstra, J.J. Beintema, Expression and characterization of active site mutants of Hevamine, a chitinase from the rubber tree *Hevea brasiliensis*, Eur. J. Biochem. 269 (2002) 893–901, https://doi.org/10.1046/j.0014-2956.2001.02721.x.
[37] H. Banani, D. Spadaro, D. Zhang, S. Matic, A. Garibaldi, M.L. Gullino, Postharvest application of a novel chitinase cloned from *Metschnikowia fructicola* and overexpressed in *Pichia pastoris* to control brown rot of peaches, Int. J. Food Microbiol. 199 (2015) 54–61, https://doi.org/10.1016/j.ijfoodmicro.2015.01.002.
[38] A.G. Hamre, S. Jana, N.K. Reppert, C.M. Payne, M. Sørlie, Processivity, substrate positioning, and binding: the role of polar residues in a family 18 glycoside hydrolase, Biochemistry 54 (49) (2015) 7292–7306, https://doi.org/10.1021/acs.biochem.5b00830.
[39] S. Jana, A.G. Hamre, V.G.H. Eijsink, M. Sørlie, C.M. Payne, Polar residues lining the binding cleft of a *Serratia marcescens* family 18 chitinase position the substrate for attack and stabilize associative interactions, Mol. Phys. 117 (23–24) (2019) 3664–3682, https://doi.org/10.1080/00268976.2019.1657600.

Glossary

GlcNAc: *N*-acetyl-D-glucosamine
GlcN: D-glucosamine
DP: degree of polymerization
CC: colloidal chitin
COS: chito-oligosaccharides
faCOS: fully acetylated COS
PEG: polyethylene glycol